DOI: https://doi.org/10.30795/jfootankle.2025.v19.1912

Original Article

Development of a novel radiographic angle to assess the calcaneal tuberosity enlargement in insertional Achilles tendinopathy

Wanjun Gu[1], Melissa L Carpenter[2], Mingjie Zhu[3], Ankit Hirpara[2], Mark S Myerson[3,4], Shuyuan Li[4,5]

1. University of California, San Francisco, San Francisco, CA, USA
2. University of Colorado School of Medicine, Denver, CO, USA
3. Department of Orthopedics, University of Colorado School of Medicine, Denver, CO, USA
4. Steps2Walk, Inc, Denver, CO, USA
5. MSK institute, Department of Surgery and Perioperative Care, Dell Medical School, University of Texas at Austin, Austin, TX, USA

Abstract

Objective: This study investigated morphologic features of the calcaneal tuberosity in a group of normal controls and developed a radiographic angular metric, the Pathologic Achilles Insertion Angle (PAIA), with the goal of assisting in the insertional Achilles tendinopathy (IAT) evaluation.

Methods: On lateral weight-bearing radiographs, calcaneal tuberosities of 33 control feet were analyzed to develop a mathematical algorithm-based Standard Circle to describe the ideal contour of each tuberosity.

Results: Offsets of the circle center and the circle radius were scaled according to their dimensions and the weight-bearing features of the calcaneus (Algorithm 1). Then, enlarged calcaneal tuberosities of 58 feet with different severities of IAT were plotted, and their respective ideal Standard Circles were generated. An angular measurement algorithm (Algorithm 2) was developed to describe how to rotate each enlarged tuberosity to align with its ideal contour using the weight-bearing point as the apex. Thus, the PAIA angular metric provided the amount of the enlargement.

Conclusion: Pathologic Achilles Insertion Angle is a novel radiographic metric that considers morphological and biomechanical features of the calcaneal tuberosity and is able to quantitatively evaluate the enlargement of the calcaneal tuberosity in IAT.

Level of evidence IV; Case series; Therapeutic studies - investigating the results of treatment.

standard

Keywords: Insertional Achilles tendinopathy; Calcaneal tuberosity; Morphology; Weight-bearing; Radiography.

Introduction

Insertional Achilles tendinopathy (IAT) is a common cause of posterior heel pain[1-3]. In a study conducted in 1995, 20% of 163 patients with chronic heel pain had IAT[4]. Six percent of the general population experience Achilles tendon pain and, of these patients, approximately one-third have IAT[2,5-8]. Similarly, Paavola et al. reported that 24.7% of patients with chronic ailment of the Achilles had an insertional Achilles pathology, with 20% of these patients having pure IAT[9,10]. The pathology of IAT includes calcification and degenerative changes of the Achilles insertion on the calcaneus[11,12]. Etiology has been found associated with overuse, mechanical overloading, and improper form when training, as well as possible stress shielding[9,13-16].

When 3–6 months of continuous conservative treatment fails, surgical management can be considered[2]. The traditional surgical intervention is calcaneoplasty, which includes resection of bone spur/calcification at the Achilles

Study Department of Orthopedics, University of Colorado School of Medicine, Denver, CO, USA.

Correspondence: Shuyuan Li. 1501 Red River St, Austin, TX, USA 78712. Steps2Walk, IncSteps2Walk, Inc. Denver, CO, USA, 80011 **Email:** drshuyuanli@gmail.com. **Conflicts of interest**: none. **Source of funding:** none. **Date received:** May 28, 2025. **Date accepted:** September 26, 2025.

How to cite this article: Gu W, Carpenter ML, Zhu M, Hirpara A, Myerson MS, Li S. Development of a novel radiographic angle to assess the calcaneal tuberosity enlargement in insertional Achilles tendinopathy. J Foot Ankle. 2025;19(3):e1912.

Copyright © 2025 - Journal of the Foot&Ankle

insertion and reattachment of the Achilles tendon with or without Achilles insertion reconstruction[17,18]. An alternative treatment is the Zadek procedure, a dorsal closing-wedge osteotomy of calcaneal tuberosity. It was first introduced in 1939, for the treatment of Achilles bursitis, and has been popularized during the past two decades in the treatment of both IAT and Haglund's deformity. It reduces the length of the calcaneus as opposed to a calcaneoplasty, i.e., removal of the osteophyte and reshaping of the calcaneal tuberosity[19-21]. Zadek osteotomy was proved to have minimal post-operative pain, swelling, scarring, and recovery time, as well as improved functional scores[22].

Despite the success of the procedures above, there is no agreement on how to correlate the size of the calcaneoplasty or the size of the Zadek osteotomy with the amount of enlargement of the calcaneal tuberosity in IAT. The present study investigated the morphological features of the calcaneal tuberosity on weight-bearing radiographs in normal controls and patients with IAT, developeing a novel angular measurement of the enlarged tuberosity in IAT with the goal of potentially assisting surgical planning.

Methods

Selection of study samples

This was an institutional review board-approved imaging study using weight-bearing radiographic images taken at a foot and ankle center for standard care purposes. Lateral view, weight-bearing radiographic images of 33 adults' feet (age > 18 years) without IAT, Haglund's deformity, a history of calcaneal trauma, or other remarkable deformities of the foot were included in the control group to study the normal morphology of the calcaneal tuberosity. Lateral view, weight-bearing radiographic images of 58 feet from adult patients with symptomatic IAT who underwent a calcaneoplasty surgery were used in the study group.

Delineating contour of control calcaneal tuberosities

The 33 control radiographs were imported into ImageJ[23,24]. Each calcaneus was circumscribed with a rectangle box such as that each side of the rectangle corresponded to the anterior, superior, posterior, and inferior border of the calcaneus. Then, 90 points were plotted onto the rectangle and calcaneus to determine dimensions and weight-bearing features (for example, weight-bearing point, declination/pitch angle) of the calcaneus and the contour of the calcaneal tuberosity (Figure 1). Among these 90 points, some were set up as calibration markers for measurement purposes (points 1–3) and others represented standardized anatomic markers, while the remainder points were randomly distributed between two adjacent anatomical markers along the contour of the bone for mapping purposes (Table 1). The weight-bearing point was defined as the point of the calcaneus in touch with the ground on the lateral view of the radiograph. In the placement of the 90 points, only 16 of them (points 1–14, 36, 90) were subjective to human errors. These were

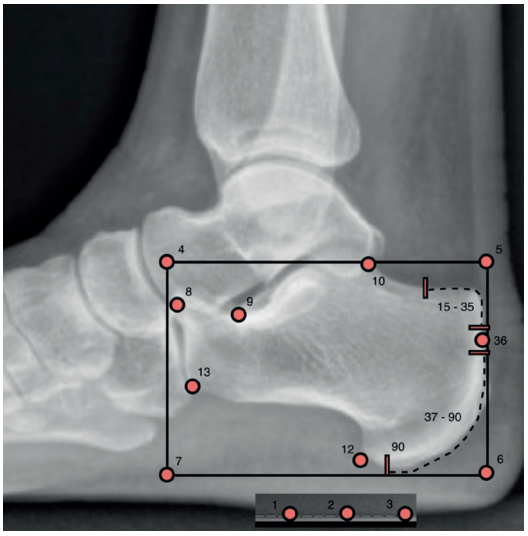

Figure 1. The calcaneus was circumscribed within a rectangle box. Points 1–3 were used for calibration purposes. Points 4–90 were plotted with some of them representing various anatomical markers, while the rest was evenly distributed to plot and map the contour of the calcaneal tuberosity.

Table 1. Significance of the 90 points used for plotting purposes

Plotting Point	Significance
1	0 cm (for measurement calibration)
2	1 cm (for measurement calibration)
3	2 cm (for measurement calibration)
4	Upper anterior corner of the rectangle circumscribing the calcaneus
5	Upper posterior corner of the rectangle circumscribing the calcaneus
6	Lower posterior corner of the rectangle circumscribing the calcaneus
7	Lower anterior corner of the rectangle circumscribing the calcaneus
8	Superior anterior point of the calcaneal anterior process
9	Apex of the Gissane angle
10	Summit of the posterior facet
11	Most superior posterior point of the calcaneal tuberosity
12	Insertion of the plantar fascia
13	Inferior anterior point of the calcaneal anterior process
14	Summit of the calcaneal tuberosity
15-35	Arising slope leading to the summit of the calcaneal tuberosity
36	Inferior point of the retrocalcaneal tendon-bone contact surface, i.e., the superior starting point of the Achilles insertion
37-89	The whole tendon-bone insertion of the Achilles on the calcaneal tuberosity
90	Weight-bearing point of the calcaneus

reviewed by two fellowship-trained orthopedic foot and ankle surgeons. There was no critical requirement of the exact distance between two adjacent non-landmark points.

Determining the individualized Standard Circle to predict the ideal calcaneal tuberosity contour

The x and y coordinates of the rectangle were characterized by point 7, denoted as the origin of the x and y coordinates, i.e., $A(0, 0)$; point 6, denoted as $B(x_B, 0)$; and point 4, denoted as $C(0, y_C)$ (Figure 2). The width and height of each rectangle were represented by x_B, y_C, while the diagonal length (D) of the rectangle was calculated using and as follows (Figure 1):

$$D = \sqrt{x_B^2 + y_C^2}$$

Using the x and y coordinates of the 90 points described above, an individualized Standard Circle was created mathematically for every calcaneal tuberosity. These were designed to delineate the best approximated contour of an "ideal" or "normal" calcaneal tuberosity considering dimensional and biomechanical features of the calcaneus. Two essential parameters were used to define the individualized Standard Circle for each calcaneal tuberosity: offsets of x and y coordinates of the circle's center, denoted as $O(x_o, y_o)$, and the radius (R) of the Standard Circle. These were indirectly determined by the calcaneus dimensions in terms of height, length, calcaneal pitch angle, etc. Then, the coordinates (x, y) of plotted points on the curvature of a control calcaneal tuberosity were standardized and approximated using the following equation to determine its individualized Standard Circle:

$$(x - x_0)^2 + (y - y_0)^2 = R^2$$
$$(x - Average\ x_0)^2 + (y - Average\ y_0)^2 = Average\ R^2$$

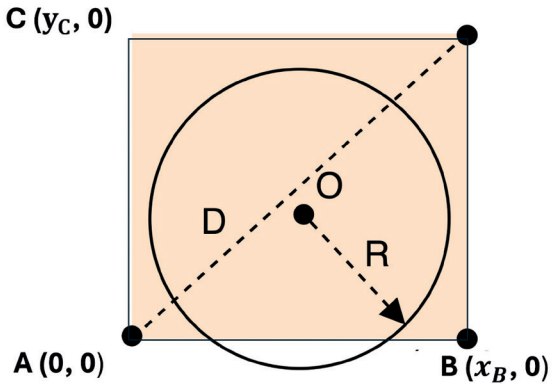

Figure 2. The fitting algorithm used a circular function with the center O and radius R. The rectangular box circumscribing each control calcaneus was denoted by diagonal length D and corner point A (0,0) (corresponding to point 7 in Figure 1), point B (, 0) (corresponding to point 6 in Figure 1), and point C (0,) (corresponding to point 4 in Figure 1).

All 33 rectangles from the 33 control calcanei were then normalized to an average square to mediate differences in foot sizes. Average values of O (x_o, y_o), and R for the 33 control calcanei were calculated statistically and turned into constant parameters ($Average\ x_0$ = 0.53, $Average\ y_0$ = 0.39, $Average\ R$ = 0.47) (see the result section). Therefore, the final algorithm for determining the individualized Standard Circle to predict the ideal calcaneal tuberosity contour of a given calcaneus, with or without IAT, is as follows:

$$(x - 0.53)^2 + (y - 0.39)^2 = 0.47^2 \text{ (**Algorithm 1**)}$$

Developing the Pathologic Achilles Insertion Angle

Calcanei of the 58 feet with IAT were circumscribed by excluding the enlargement in the calcaneal tuberosity. Ninety points were plotted. Points 1–36 were used to collect the dimensional information of each calcaneus (Figure 3A), while points 37–90 were used to delineate and collect information on the enlarged calcaneal tuberosity (purple line in Figure 3A). Using this information, the Standard Circle of each calcaneus in the IAT group was calculated. Then, these enlarged calcaneal tuberosity curves were rotated using the weight-bearing point (point 90) as the apex, i.e., rotating the center to best align with their respective Standard Circles ("ideal" curvatures) using mathematical optimization. Optimization was done by projecting the y coordinate value of points 37–90 on the enlarged posterior tuberosity onto the Standard Circle of each calcaneus. In this transformation, the Standard Circle, upon projection, can be written as:

$$SC = \begin{bmatrix} SC_x \\ SC_y \end{bmatrix} = \begin{bmatrix} \sqrt{R^2 - (y_i - y_o)^2} + x_o \\ y_i \end{bmatrix}$$

where and represent the SC_x and SC_y coordinates of all the points on the Standard Circle. The x coordinate of the projected Standard Curve can be expressed as a function of the y coordinate. Rotational loss, a mean square error measuring differences between the enlarged calcaneal tuberosities and the Standard Circles of these calcaneal tuberosities in the IAT group, was minimized during the optimization. The most optimum rotation angle was worked out during the optimization (Figure 3B). This rotation angle was named Pathologic Achilles Insertion Angle (PAIA) because it represented exactly the enlargement of the calcaneal tuberosity in a foot with IAT, as well as the angle by which the enlarged calcaneal tuberosity curve can be rotated around the weight-bearing point to best fit the ideal contour predicted by the Standard Circle of that individual calcaneus.

Mathematically, the counterclockwise -angled rotation of the enlarged tuberosity can be written as:

$$RV_\theta = \begin{bmatrix} RV_{\theta x} \\ RV_{\theta y} \end{bmatrix} = \begin{bmatrix} cos\theta & -sin\theta \\ sin\theta & cos\theta \end{bmatrix} \begin{bmatrix} x_i \\ y_i \end{bmatrix} = \begin{bmatrix} x_i cos\theta - y_i sin\theta \\ x_i sin\theta + y cos\theta \end{bmatrix}$$

where RV_θ is the contour of the enlarged calcaneal tuberosity after being rotated to fit the Standard Circle, with x coordinating $RV_{\theta x}$, and y coordinating $RV_{\theta y}$, and x_i and y_i are the coordinates for the original enlarged tuberosities. Then, the rotation loss with respect to θ is quantified as a

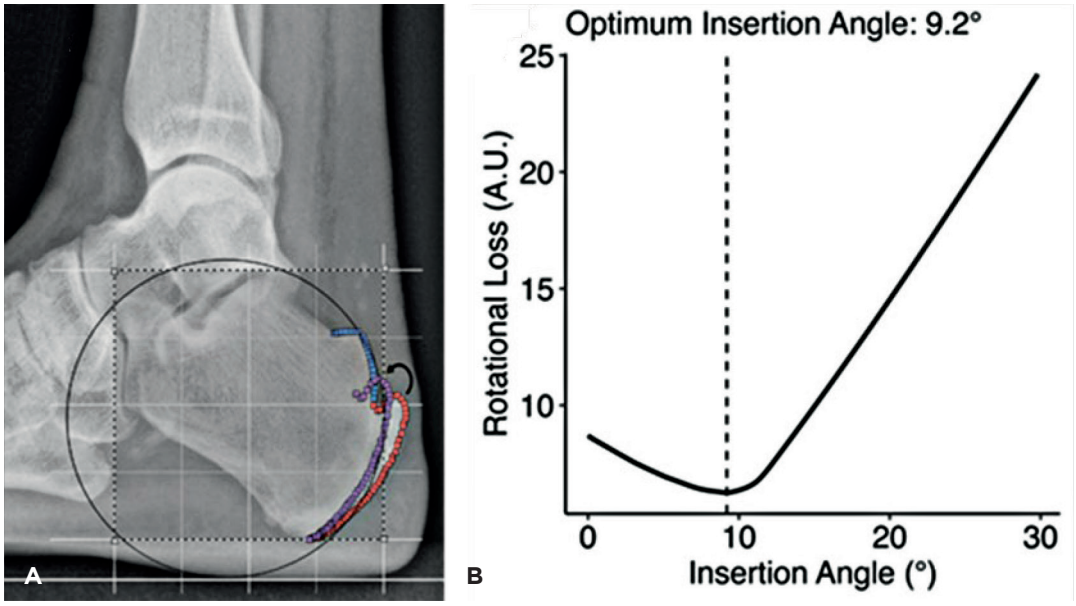

Figure 3. In 3A, blue dots represent the superior section of the calcaneus, red dots outline the enlarged calcaneal tuberosity with the Achilles insertion, and purple dots represent the rotated/realigned calcaneal tuberosity to best fit the Standard Circle of the calcaneus. 3B demonstrates the change of the rotational loss while rotating the enlarged calcaneus tuberosity to its ideal contour on the Standard Circle. The PAIA was determined at the insertion angle associated with the local minima of the rotation loss.

sum of square loss $SSE(\theta)$ which can be used to determine the similarity between the θ-rotated curvature and the Standard Circle. The $SSE(\theta)$ is defined as:

$$SSE(\theta) = \sum_{i=1}^{N} \frac{1}{N} \sqrt{(SC_{xi} - RV_{\theta xi})^2 + \left(SC_{yi} - RV_{\theta yi}\right)^2}$$

where SC_{xi}, SC_{yi} are the x and y coordinates of the Standard Circle, and $RV_{\theta xi}$, $RV_{\theta yi}$ are the x and y coordinates of the enlarged contour. The N is set to 54 because, from point 37 to point 90, 54 points in total were used to depict the enlarged contour.

The most optimum rotation angle can be found at the minimum of the rotation loss with respect to the rotation angle, or when:

$$\frac{\partial SSE(\theta)}{\partial \theta} = 0$$

The three equations above form **Algorithm 2**. The RV_θ calculates the relationship between the calcaneal tuberosity contour (points 37–90) before and after the rotation. The $SSE(\theta)$ calculates differences between the SC and RV. The third equation aims to find the θ at which the SSE (sum of squared error) is minimized. At this moment, the value of θ is the closest to its most ideal value, i.e., the PAIA. The closest the θ is to the minimal $SSE(\theta)$ (precisely to 0.001), the better the contour re-alignment is to the Standard Circle.

Theoretically, since the ideal normal contour and the enlarged contour of the calcaneal tuberosity share the same center of rotation at the weight-bearing point of the calcaneus, the PAIA size would be the size of the tuberosity enlargement when surgically reshaping the calcaneal tuberosity is considered.

Results

Demographics of the two groups

Basic demographics were summarized in Table 2. In the 33 control feet (average age 51.12 +/- 11.30 years old), 9 feet were from males and 24 feet were from females; and 31 feet were from White/Caucasian patients, 1 foot from a Black/African American patient, and 1 foot from an Asian patient. In the 58 feet with symptomatic IAT (average age 55.90 +/- 10.00 years old), 22 feet were from males and 36 feet were from females; and 56 feet were from White/Caucasian patients and 2 feet were from Black/African American patients.

Constant parameters used in algorithm 1 to determine the individualized Standard Circle

The constant parameters used in the Standard Circle **Algorithm 1** were average values generated from the 33 control calcanei. The $Average\ x_0$ was 0.53 +/- 0.07, $Average\ y_0$ was 0.39 +/- 0.03, and $Average\ R$ was 0.47 +/- 0.06. Therefore, for any calcaneus with or without IAT, upon standardizing its width and height according to calibration, it's individualized Standard Circle can be written as:

$$(x - 0.53)^2 + (y - 0.39)^2 = 0.47^2 \text{ (Algorithm 1)}$$

Table 2. Demographics of the two groups

Group	Sample size	Age		Sex		Laterality		Ethnicity		
		Mean	SD	Male	Female	Left	Right	White/Caucasian	Black/African American	Asian
Control	33	51.12	11.30	9	24	12	21	31	1	1
Study	58	55.90	10.00	22	36	31	27	56	2	0

Values of PAIA in the IAT group

In the IAT group, PAIA averaged around 15.23 +/- 4.75 degrees (Median: 13.89 degrees, Q1: 11.89 degrees, Q3: 16.33 degrees; Range: 10.03–29.29 degrees, 95% Confidence Interval: (13.98, 16.48) degrees).

Application of PAIA

Based on the algorithms above, an open access application was created to allow any user to calculate the PAIA using lateral radiographic images. The application can be accessed at https://steps2walk.shinyapps.io/paia/. Further instructions can be found at https://github.com/Steps2Walk/paia/.

Discussion

The present study introduced a novel angle based on mathematical algorithms to quantitatively determine the enlargement of the calcaneus tuberosity in IAT.

In the past, multiple imaging modalities were used to investigate a possible correlation between the calcaneus morphology and IAT, including the Fowler-Philip angle[25], Ruch calcaneal pitch angle[26], Chauveaux angle[27], and Heneghan-Pavlov parallel pitch lines[28]. However, these parameters were proven to have poor specificity and reliability, and do not incorporate the length of the calcaneus[19,20]. Tourné et al.[20] subsequently devised the radiographic X/Y ratio to aid in determining surgical indications for patients with Haglund syndrome, as well as IAT. In that measurement, X represents the calcaneal length, and Y represents the greater tuberosity length on lateral weight-bearing radiograph. They found that an X/Y ratio below 2.5 effectively differentiated patients with Haglund syndrome from those without it. In other words, a calcaneus with an X/Y ratio of less than 2.5 could be deemed "long" and, therefore, has the potential to cause impingement and excessive tension on the Achilles insertion[20]. Following that logic, patients with Haglund syndrome and X/Y ratio of less than 2.5 would likely benefit more from a Zadek osteotomy to reduce the length of the calcaneus as opposed to a calcaneoplasty, i.e., simple removal of the Haglund's deformity[19-21].

In our morphology study of the calcaneal tuberosity, several features of the calcaneus were directly or indirectly taken into consideration, including height and length, the calcaneal pitch angle, particular severity of the enlargement, and the "ideal" contour without IAT. The PAIA concept presents a significant potential advancement in the diagnosis and surgical treatment of IAT by offering a highly individualized evaluation method that considers the unique calcaneal shape of each foot. In this study, although there was a large variety of enlargement severity in the IAT group (range, 10.03–29.29 degrees), PAIA's algorithm provided the ability to calculate the enlargement angle to best fit the individual Standard Circle.

Moreover, in terms of surgical treatment of IAT, despite the satisfactory outcomes of calcaneoplasty or Zadek osteotomy, how to determine the size of the piece of bone that needs to be removed has remained uncertain or challenging. No prior studies addressed the design of the calcaneoplasty or Zadek osteotomy, not to mention to associate it with the severity of the calcaneal tuberosity enlargement in IAT. Traditionally, osteotomy's dimensions have been roughly determined by the surgeon's intuition and experience. This can lead to inconsistency and confusion among surgeons. The new angular metric PAIA introduced in this study has the potential to address this issue by normalizing the contour of the enlarged calcaneal tuberosity based on each patient's specific calcaneal dimensions.

The present study has a few limitations. Firstly, there is no reference in the literature to be used for a power analysis to determine sample size. Given the exploratory nature of this research, determining an optimal sample size for studying the morphology of the control calcaneal tuberosity group was challenging. Theoretically, a sample size of 33 patients is considered statistically modest if the control group cannot accurately reflect the overall population distribution or if outliers exist within controls. Despite this concern, Figure 4 demonstrates that the calcaneal tuberosities of the control feet are closely clustered, with no distinct outliers, suggesting that control samples may adequately represent normal calcaneal tuberosities. Considering the limited sample size in terms of sex, age, and ethnicity, this new angular measurement needs to be tested in future studies. Secondly, there was no reliability measurement (intraclass correlation, ICC) due to the lack of prior reference data that could be used as a golden standard compared with PAIA. During the development of these algorithms, in the placement of the 90 points, only 16 of them (points 1–14, 36, 90) were subjected to human errors. These were reviewed by two fellowship-trained orthopedic foot and ankle surgeons. There was no critical requirement of the exact distance between two adjacent non-landmark points. As described, once the initial landmarks were placed, algorithms generated a PAIA automatically. This step had almost no potential for error. Moreover, the

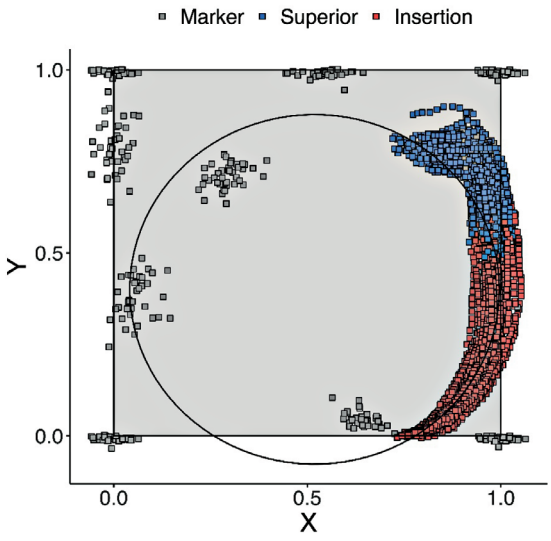

Figure 4. Average Standard Circle statistically fitted using plotted calcaneal tuberosities from 33 control calcanei. Gray dot clusters represent the preliminarily plotted anatomical markers (see Table 1 for their different significances). Blue dots represent the superior section of the calcaneal tuberosity that is not part of the Achilles insertion. Red dots represent the Achilles insertion section. Details about these plotted points are described in Table 1.

distribution of the control group provided indirect evidence of robustness. As shown in Figure 3, calcaneal tuberosities of the control feet cluster tightly, with minimal scatter and no discernible subgroups, suggesting that the selected sample adequately reflected the spectrum of the normal controls. We believe that, in this context, this clustering pattern can empirically reflect a low variance and supports the adequacy of the sample, mitigating concerns regarding hidden biases or uncontrolled variability. Future studies with larger, more diverse populations may allow formal reliability testing. Thirdly, the PAIA was developed using only morphological data of the calcanei on lateral radiographs, a limited two-dimensional single view. Morphological metrics in other planes and the alignment of the whole foot, including hindfoot alignment and arch height, have been shown in some preliminary studies to correlate with IAT. These may also influence the biomechanics of IAT and the design of the calcaneoplasty or Zadek osteotomy accordingly. However, one must recognize that, if too many parameters are considered in the design of a metric, it will compromise ease-of-use, increase noise, and reduce precision and specificity. Nonetheless, one must acknowledge that two-dimensional weight-bearing lateral view radiograph is the current standard of practice globally. Lastly, this study provides a preliminary concept of restoring the enlarged calcaneal tuberosities to their normal contours in treating IAT surgically; however, the clinical utility of this theory needs to be validated in future clinical and biomechanical studies.

The present paper introduced an easy-to-use mathematical model with the potential of guiding the surgical planning of a Zadek osteotomy. There is potential to create patient-specific three-dimensional guides using the same concept of restoring an enlarged calcaneal tuberosity to a more normal range. The authors would like to point out that this was a preliminary study based on measurements of two-dimensional weight-bearing lateral view radiographs. Extrapolation of these findings needs to be substantiated in future prospective studies, clinical validation, and multicenter trials.

Conclusion

The PAIA is a novel angle which takes the morphology of the calcaneus into consideration to quantitatively evaluate the enlarged calcaneal tuberosity in IAT. Further biomechanical, cadaveric, and clinical studies are needed to prove the concepts above and their clinical utility.

Authors' contributions: Each author contributed individually and significantly to the development of this article: WG (https://orcid.org/0000-0002-7342-7000) Conceived and planned the activity that led to the study, wrote the article, participated in the review process; VL *data collection, bibliographic review; MZ *(https://orcid.org/0000-0002-9685-4048) formatting of the article, bibliographic review; AH * interpreted the results of the study, participated in the review process; MSM (https://orcid.org/0000-0001-5124-2403), and SL (https://orcid.org/0000-0003-1238-8455) Performed the surgeries; data collection, statistical analysis. All authors read and approved the final manuscript. *ORCID (Open Researcher and Contributor ID).

References

1. Moonot P, Dakhode S. Current concept review of Achilles tendinopathy. J Clin Orthop Trauma. 2024;50:102374.
2. Chimenti RL, Cychosz CC, Hall MM, Phisitkul P. Current Concepts Review Update: Insertional Achilles Tendinopathy. Foot Ankle Int. 2017;38(10):1160-9.
3. Ferguson A, Christophersen C, Elattar O, Farber DC. Achilles Tendinopathy and Associated Disorders. Foot & Ankle Orthopaedics. 2019;4(2):2473011419838294.
4. Aström M, Rausing A. Chronic Achilles tendinopathy. A survey of surgical and histopathologic findings. Clin Orthop Relat Res. 1995(316):151-64.
5. Karjalainen PT, Soila K, Aronen HJ, Pihlajamäki HK, Tynninen O, Paavonen T, et al. MR imaging of overuse injuries of the Achilles tendon. AJR Am J Roentgenol. 2000;175(1):251-60.
6. Khan KM, Forster BB, Robinson J, Cheong Y, Louis L, Maclean L, et al. Are ultrasound and magnetic resonance imaging of value in assessment of Achilles tendon disorders? A two year prospective study. Br J Sports Med. 2003;37(2):149-53.
7. Kujala UM, Sarna S, Kaprio J. Cumulative incidence of achilles tendon rupture and tendinopathy in male former elite athletes. Clin J Sport Med. 2005;15(3):133-5.
8. Nicholson CW, Berlet GC, Lee TH. Prediction of the success of nonoperative treatment of insertional Achilles tendinosis based on MRI. Foot Ankle Int. 2007;28(4):472-7.
9. Krishna Sayana M, Maffulli N. Insertional Achilles tendinopathy. Foot Ankle Clin. 2005;10(2):309-20.
10. Paavola M, Orava S, Leppilahti J, Kannus P, Järvinen M. Chronic Achilles tendon overuse injury: complications after surgical treatment. An analysis of 432 consecutive patients. Am J Sports Med. 2000;28(1):77-82.
11. Li HY, Hua YH. Achilles Tendinopathy: Current Concepts about the Basic Science and Clinical Treatments. Biomed Res Int. 2016;2016:6492597.
12. Maffulli N, Saxena A, Wagner E, Torre G. Achilles insertional tendinopathy: state of the art. Journal of ISAKOS. 2018;4(1):48-57.
13. Myerson MS, McGarvey W. Disorders of the Achilles tendon insertion and Achilles tendinitis. Instr Course Lect. 1999;48:211-8.
14. Schepsis AA, Jones H, Haas AL. Achilles tendon disorders in athletes. Am J Sports Med. 2002;30(2):287-305.
15. Benjamin M, Evans EJ, Copp L. The histology of tendon attachments to bone in man. J Anat. 1986;149:89-100.
16. Rufai A, Ralphs JR, Benjamin M. Structure and histopathology of the insertional region of the human Achilles tendon. J Orthop Res. 1995;13(4):585-93.
17. Barg A, Ludwig T. Surgical Strategies for the Treatment of Insertional Achilles Tendinopathy. Foot Ankle Clin. 2019;24(3):533-59.
18. Chen J, Janney CF, Khalid MA, Panchbhavi VK. Management of Insertional Achilles Tendinopathy. J Am Acad Orthop Surg. 2022;30(10):e751-e9.
19. Tourne Y, Baray AL, Barthelemy R, Karhao T, Moroney P. The Zadek calcaneal osteotomy in Haglund's syndrome of the heel: clinical results and a radiographic analysis to explain its efficacy. Foot and Ankle Surgery. 2022;28(1):79-87.
20. Tourné Y, Baray AL, Barthélémy R, Moroney P. Contribution of a new radiologic calcaneal measurement to the treatment decision tree in Haglund syndrome. Orthop Traumatol Surg Res. 2018;104(8):1215-9.
21. Tourné Y, Francony F, Barthélémy R, Karhao T, Moroney P. The Zadek calcaneal osteotomy in Haglund's syndrome of the heel: Its effects on the dorsiflexion of the ankle and correlations to clinical and functional scores. Foot Ankle Surg. 2022;28(6):789-94.
22. Poutoglidou F, Drummond I, Patel A, Malagelada F, Jeyaseelan L, Parker L. Clinical outcomes and complications of the Zadek calcaneal osteotomy in Insertional Achilles Tendinopathy: A systematic review and meta-analysis. Foot Ankle Surg. 2023;29(4):298-305.
23. Schindelin J, Arganda-Carreras I, Frise E, Kaynig V, Longair M, Pietzsch T, et al. Fiji: an open-source platform for biological-image analysis. Nature methods. 2012;9(7):676-82.
24. Schneider CA, Rasband WS, Eliceiri KW. NIH Image to ImageJ: 25 years of image analysis. Nature methods. 2012;9(7):671-5.
25. Thomas JL, Christensen JC, Kravitz SR, Mendicino RW, Schuberth JM, Vanore JV, et al. The diagnosis and treatment of heel pain: a clinical practice guideline–revision 2010. The Journal of Foot and Ankle Surgery. 2010;49(3):S1-S19.
26. Lu C-C, Cheng Y-M, Fu Y-C, Tien Y-C, Chen S-K, Huang P-J. Angle Analysis of Haglund Syndrome and its Relationship with Osseous Variations and Achilles Tendon Calcification. Foot & Ankle International. 2007;28(2):181-5.
27. Taylor GJ. Prominence of the calcaneus: is operation justified? J Bone Joint Surg Br. 1986;68(3):467-70.
28. Heneghan MA, Pavlov H. The Haglund painful heel syndrome experimental investigation of cause and therapeutic implications. Clinical Orthopaedics and Related Research®. 1984;187:228-34.